Heat Release Mechanisms in Inhibited Laminar Counterflow Flames

KI YONG LEE, DON J. CHA, ANTHONY HAMINS, and ISHWAR K. PURI*

Department of Mechanical Engineering (M/C 251)
University of Illinois at Chicago, Chicago, Illinois 60607-7022 (K.Y.L.; D.J.C.; I.K.P.)
and Building and Fire Research Laboratory, National Institute of
Standards and Technology, Gaithersburg, Maryland 20899 (A.H.)

Due to the participation of inhibitors in flame chemistry, it is difficult to concurrently characterize the complex interaction between their cooling action and chemical inhibition (which decrease temperature), and their contribution of heat release (which increases temperature). Investigations involving chemical inhibitors have to contend with three interacting phenomena, i.e., (1) the cooling action due to the specific heat of the species; (2) the heat release due to their burning; and (3) inhibition associated with scavenging of critical radical species. This study investigated the effect of chloromethane (a chemical inhibitor due to its halogenation) on the heat release in methane–air nonpremixed flames. For comparison, the effect on the heat release due to the purely thermal action of nitrogen (which does not exhibit chemical inhibition or heat release effects) was also investigated. The flames were experimentally and numerically studied in a counterflow configuration, and the heat release was calculated from simulations involving detailed chemistry. When inert suppressants were added to the oxidizer stream of a nonpremixed flame, the global heat release decreased. Chloromethane addition to the fuel stream, however, increased the heat release. Whereas addition of nitrogen narrowed the heat release region, chloromethane addition to the oxidizer altered the flame stoichiometry, such that the heat release profiles were markedly different. Halogenated compounds can influence radiative thermal losses from flames through changes in flame structure that effect the temperature and soot concentration. Therefore, a small Schmidt–Boelter type gauge was used to measure the radiative flux through a cylindrical control volume surrounding the flame, and the total radiation emitted from the flame was calculated by integrating the emitted flux. The results show that as nitrogen was added to the methane–air base flame, the radiative heat loss fraction decreased slightly. When chloromethane was added to the oxidizer stream, the radiative heat loss fraction increased substantially ($\approx 40\%$). Values of the radiative heat loss fraction remained relatively small (≈ 2-3%) for all of the flames studied.

INTRODUCTION

Fundamental investigations of chemical inhibitors are necessarily limited to those substances whose participation in hydrocarbon chemistry is relatively well characterized by detailed chemical kinetic mechanisms. Chemical inhibitors for which detailed chemical kinetic information is available are the simpler halogenated hydrocarbons such as chloromethane [1–4]. Some simple halogenated species react with oxygen at high temperatures, behaving not unlike fuels. Thus, investigations involving halogenated agents have to unravel three interacting phenomena, i.e., (1) cooling due to the specific heat of the species; (2) heat release due to their burning; and (3) scavenging of critical radical species. These interactions are complex and are coupled.

To better understand the mechanism of flame inhibitors, both the kinetic and thermal channels of inhibition must be simultaneously characterized. From the perspective of flame stability, it is important to identify the influence of chemical agents on flame heat release. Flame extinction occurs when heat losses exceed heat generation. For instance, thermal inhibitors cool flames through heat capacity effects, whereas chemical inhibitors simultaneously cool flames through heat capacity effects and reduce radical superequilibrium concentrations.

The inhibition of critical radical species due to thermal and chemical inhibitors has been the focus of an earlier investigation in our laboratories [5]. In that study, attention was focused on the detailed temperature, species, and velocity profiles in inhibited flames. Veloc-

*Corresponding author.

COMBUSTION AND FLAME 104: 27–40 (1996)

Published by Elsevier Science Inc.

0010-2180/96/$15.00
SSDI 0010-2180(95)00105-F

ity and temperature measurements in the counterflow flames were used to validate the computational flame model [5–7]. In this study attention is focused on the heat release and its form, in both inhibited and noninhibited counterflowing flames.

A thorough investigation of flame stability must consider the importance of heat losses through radiative emission. Halogenated compounds can influence radiative emission through changes in flame structure including increases in the temperature field and soot concentration. Inherent in nearly all calculations involving counterflow flames has been the assumption that radiative emission from the flame is negligible. Nonnegligible radiative emission will impact the temperature and species profiles determined from the numerical models. Concern about the issue of radiative loss near extinction in nonpremixed counterflow flames prompted the development of an asymptotic theory of flame structure that includes thermal radiation [11]. In that study radiative losses were considered to be relatively small compared with the heat release established at conditions near extinction. In a separate study, the radiative heat transfer from a "cylindrical" counterflow flame was determined by integrating the heat and mass transfer equations using measured flame structure data and estimated soot volume fractions [12]. Recently, detailed radiative emission calculations that include contributions due to both particulates and gas band emission in counterflow flames have been reported [13–15]. The flames involving chloromethane studied here are characterized by a yellow luminosity, calling into question the relative importance of thermal radiation in the simulations [5, 6]. Thus, measurements are made to determine the magnitude of radiative losses from these counterflow flames.

Counterflow flames result when two axisymmetric reactant streams flow towards each other in a stagnation point flow. These flames are well suited for the investigation of flame structure since the stretch rate, which defines the flowfield, is an independently controlled parameter. In the case of laminar flows, the resulting flame structure is steady and one-dimensional with respect to temperature and species concentrations. The structure of counterflowing flames has been extensively studied using numerical codes which integrate the conservation equations and include detailed models of molecular transport and chemical kinetics [8–10]. Use of these models has focused on a number of applications including flame stability and pollutant formation. A wide variety of fuel types (methane, chloromethane, heptane, hydrogen, to name a few) and flame configurations (nonpremixed, partially premixed, and premixed) have been investigated. Therefore, these flames are attractive from the perspective of investigating flame inhibition phenomena.

OBJECTIVES

The objectives that motivated this investigation were as follows:

1. The effect of inhibitors on the structure of hydrocarbon flames was the focus of study to gain insight into the complex interactions that impact the global heat release in flames and, ultimately, flame stability, since chemical inhibition may manifest itself through decreases in key radical species concentrations, alteration of the flame heat release profiles, and/or by changes in radiative emission.
2. A second objective was to develop a methodology for the measurement of radiative emission from counterflowing flames, and to compare the impact of suppressants on the radiative heat loss emitted from a flame.

METHODOLOGY

Laminar counterflow flames established under atmospheric conditions were investigated. An uninhibited methane–air "base" flame was compared with flames that were inhibited by adding molecular nitrogen and chloromethane to the oxidizer stream. In one additional case, chloromethane was added to the fuel stream. Nitrogen behaves as a thermal inhibitor when added to flames, whereas chloromethane has a combination of physical and chemical behavior [5]. The physical behavior of N_2 is manifest by its thermal cooling of flames, causing a de-

crease in key reaction rates which impact the heat release. Therefore, no significant differences in flame stability are expected if nitrogen is added to either the fuel or oxidizer stream as long as "accessibility" to the flame is considered. In contrast, CH_3Cl exhibits different chemical kinetic behavior when added to the fuel or oxidizer stream due to the reactivity of chloromethane. When CH_3Cl is added to the oxidizer stream, inhibition effects are due to the formation of a premixed type reaction zone, whereas addition of this species to the fuel stream involves combustion of a nonpremixed flame with two initially distinct fuels. In the study reported here, chloromethane addition to the fuel stream of a methane–air flame was also investigated.

Chemistry–Flow Interaction

The coupling that exists between a flame and the flowfield is of fundamental importance to combustion processes. One flame-flowfield interaction is the response of a flame to a straining flowfield. This is often characterized through a single parameter, i.e., the Damköhler number [16]. In counterflowing streams, a flame is established at a fixed fluid dynamic stretch rate and the reactant composition can be changed to investigate effects that arise due to the flame chemistry [5]. Therefore, for each flame discussed here, the stretch rate was maintained constant by adjusting the mass fluxes in a counterflow to analyze significant elements of the inhibition-related chemistry in equivalent flowfields. Since there are distinct stretch rates corresponding to different regions in a flame, the stretch rate referred to here is the gradient of the axial velocity on the oxidizer side of the high temperature reaction zone [5, 6, 17].

Burner

Atmospheric laminar counterflow flames were established in a burner that has been previously described [5]. Disturbances due to radiative flux transducers positioned inside the ducts were minimized by increasing all burner dimensions by a factor of 2.0 from those reported in Refs. 5–7. The burner consisted of two opposed ducts placed 15 mm apart. The ducts, with a 48 mm inner diameter, contained several fine wire mesh (50 mesh/in) screens near the duct exits (the same mesh size used for all flame conditions), a standard technique causing the flow to be laminar [18, 19]. The reactant streams were metered through calibrated flowmeters. A co-annular flow of nitrogen isolated the flames from ambient disturbances. The diameter of the visible flames, upon introduction of the nitrogen curtain, was 82 mm in all cases.

Conditions

Oxidizer-Size Inhibition. Measurements showed that at a stretch rate corresponding to $\approx 98\ s^{-1}$, 14.1% (by volume) nitrogen or 9.6% chloromethane must be added to the oxidizer stream of the methane-air flame to extinguish it. Five flames established at a stretch rate of $98\ s^{-1}$ were investigated including (1) a methane-air "base" flame; and the methane base flame inhibited by addition of (2) 6.6% excess nitrogen (by volume), (3) 13% excess nitrogen, (4) 5% chloromethane; and (5) 9% chloromethane. Flames 1–3 were visibly blue indicating the absence of a substantial amount of soot, whereas flames 4 and 5 were yellowish on the fuel side and blue on the oxidizer side of the high temperature reaction zone. Flame 1 represented vigorous burning conditions. Flames 3 and 5 were close to extinction, whereas flames 2 and 4 were established at conditions intermediate between vigorous burning and extinction.

Fuel-Side Inhibition. A flame with 50% chloromethane by volume added to the fuel stream extinguished at a critical stretch rate corresponding to $\approx 160\ s^{-1}$. Therefore, a sixth inhibited flame with 50% CH_3Cl by volume added to the fuel stream to the methane-air flame was also established at a stretch rate of $\approx 98\ s^{-1}$, i.e., relatively close to extinction.

Numerical Method

Numerical simulations of strained nonpremixed flames were performed using a previ-

ously developed computer code [10] that employs a detailed model of the molecular transport of chemical species, as well as detailed chemical reaction schemes [20]. The chemical kinetic scheme was taken from the literature [4, 21]. The kinetic mechanism includes 357 elementary forward and backward reactions, and involves 38 gas-phase species, including C_2 chlorinated and nonchlorinated hydrocarbons. Further details of the calculation methodology are described in Refs. 5 and 22. For convenience, the reaction numbers referred to here correspond to those employed previously [5, 22].

Radiation

The radiative heat loss fraction χ_R is the ratio of the radiative enthalpy emission rate from a flame Q_{rad} taken with respect to the idealized combustion heat release rate Q_{chem}. χ_R values on the order of 0.01 to 0.06 have been predicted depending on the global flow field strain rate in high pressure and atmospheric counterflowing methane-air nonpremixed flames [14, 15]. For a steady nonpremixed flame in a typical configuration, such as that involving a pool or jet, χ_R is experimentally determined by measuring the mass burning rate and the radiative heat loss rate through a control surface surrounding the flame [23, 24]. In jet flames χ_R depends on both fuel type and total heat release. Methane jet flames, for example, have χ_R values between 0.05 and 0.30 for 5–70 kW heat release flames [23].

The radiative heat flux emitted by the flames was measured using a small water-cooled Schmidt-Boelter gauge at locations on a cylindrical surface surrounding the flame. The gauge had a 6.35 mm outer diameter, a flat spectral response, and a view angle of 150°. The transducer was calibrated using a tungsten lamp and a reference gauge traceable to NBS standards. A hole corresponding to the gauge O.D. was cut into the screens to accommodate the transducer which was inserted into either duct such that its face was flush with the screens. The gauge was water cooled with a tube extracted through the base of the ducts. A schematic diagram of the burner and measurement assembly is presented in Fig. 1.

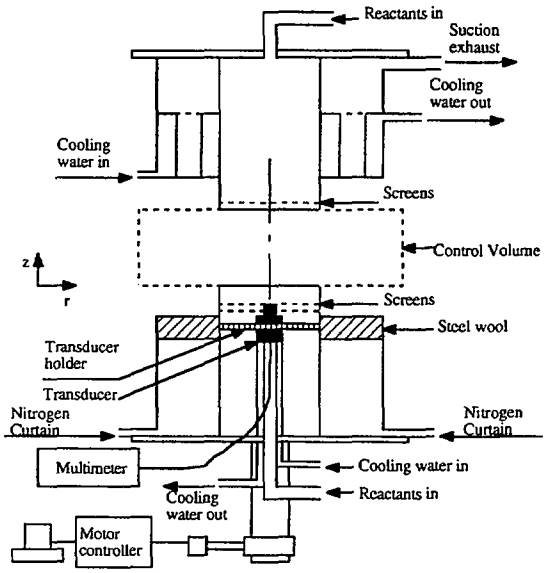

Fig. 1. Schematic diagram of the burner and measurement assembly. The drawing is not to scale.

Under conditions of high radiative heat flux, heat transfer from the gauge face to a passing fluid is possible due to high temperature of the gauge face. Noncombusting experiments with an infrared heat lamp showed that convective transfer from the face of the gauge to the reactant streams was negligible. An uncertainty estimate of 10% for the radiative flux measurements was determined from an error analysis.

Radiative Heat Flux Measurements

The gauge was placed at the periphery of the control volume as shown in the schematic diagram presented in Fig. 2. For certain cases, when the transducer was placed inside either duct, it was observed to visibly distort the flame. For these situations, the transducer and screens were moved back inside the duct until the malformation disappeared. Two typical displacement values, of 5.3 mm (Case I), and 12.8 mm (Case II), were found sufficient to provide undisturbed flames for the conditions investigated. These cases are illustrated in Fig. 2. Measurement of the radiative flux to the plane of the duct were made at the centerline of symmetry and at two radial positions (12.7 and 41 mm). Since the measurement location at 41

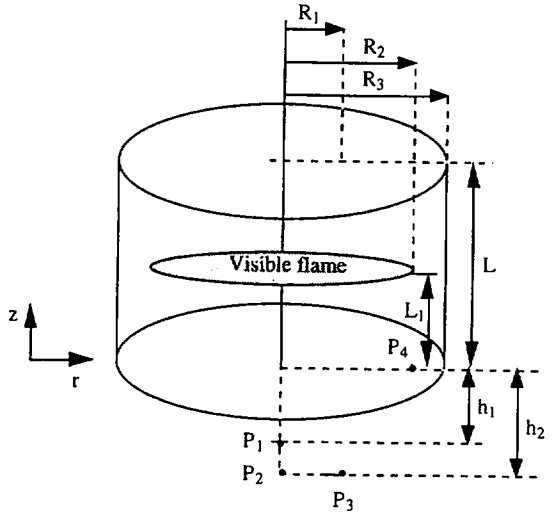

R_1 = off center radial location, 12.7 mm
R_2 = visible flame radius, 41 mm
R_3 = location of axial measurements, 60 mm

h_1 = vertical distance from duct (= 5.3 mm), Case I
h_2 = vertical distance from duct (= 12.8 mm), Case II

P_1 = Case I (location of gauge on centerline)
P_2 = Case II (location of gauge on centerline)
P_3 = Case II (location of gauge on off-center)
P_4 = Location (at R_2) of gauge flush with duct

L = Duct separation distance, 15 mm
L_1 = Distance of visible flame from oxidizer duct

Fig. 2. Schematic diagram of the control volume employed to make measurements of the radiative flux. The measurement locations corresponding to Case I and Case II are also shown.

mm from the axis of symmetry was outside the duct, introduction of the transducer at that station had a negligible effect on the flowfield, allowing placement of the transducer face flush with the duct exit plane. Measurements of radiative emission from the sides of the cylindrical control volume were made at 24 vertical locations at a distance R_3 (= 60 mm) with the gauge oriented towards the axis of symmetry. The flow and measurement conditions are listed in Table 1.

Radiative Heat Flux Corrections

Measurements made with the transducer placed in the duct interior were corrected to obtain the heat flux out of the control volume, i.e., at the duct exit plane (see Fig. 2). All of the emitted radiation was assumed to originate from the surface of the visible flame zone which was modeled as a radiating disk. Configuration factors obtained from Ref. 25 were employed. This assumption is reasonable, since effects due to flamelet thickness on thermal radiation are important only for flames at low strain rates [13]. In addition, since no significant radiative absorption occurred due to methane, air–nitrogen, or air–chloromethane mixtures, a view factor correction was suitable. The moderate strain rate at which the flames were investigated was motivated in part to obtain sufficiently optically thin flames to which application of the configuration factor correction was appropriate.

TABLE 1

The Flow and Measurement Conditions for the Five Different Flames Studied[a]

Flame	V_F (m s^{-1})	V_O (m s^{-1})	Centerline O	Centerline F	Off center O	Off center F
(1) CH_4–Air	0.74	0.68	I	II	II	II
(2) +6.6% N_2	0.74	0.70	I	II	II	II
(3) +13% N_2	0.74	0.72	I	II	II	II
(4) +5% CH_3Cl	0.76	0.65	I	II	II	II
(5) +9% CH_3Cl	0.77	0.63	II	II	II	II

[a] The fuel duct velocity is denoted by V_F and the oxidizer duct velocity by V_O, and O and F respectively denote the oxidizer and fuel sides. The measurement condition refers to either of Case I or II referred to in the text.

The experimental control volume was defined as a cylinder 120 mm in diameter and 15 mm in length. When the transducer was embedded inside the duct on the axis of symmetry, the relevant configuration factor was that of a disk parallel to a coaxial disk of unequal radius [25]:

$$F_{1-2} = 0.5\left[X - \sqrt{X^2 - 4(R_2/R_1)^2}\right], \qquad (1)$$

where F_{1-2} denotes the configuration factor, R_1 and R_2, respectively, equal (r_1/h) and (r_2/h) (with r_1 and r_2 representing the radii of the visible flame and the transducer, respectively, and h the distance between the trans-

ducer and the visible flame), and $X \equiv [1 + (1 + R_2^2)/R_1^2]$. The symbols 1 and 2, respectively, refer to the flame and the transducer. Similarly, when the transducer was offset a distance a from the centerline, the relevant configuration factor was for a plane element with respect to a circular disk in a plane normal to the element, with the normal to the element now no longer passing through the disk center [25]. The equation describing the factor is:

$$F_{1-2} = 0.5\left[1 - (Z - 2R^2)/(Z^2 - 4R^2)^{1/2}\right] \times \frac{A_2}{A_1}, \quad (2)$$

where $Z = 1 + H^2 + R^2$, and H and R, respectively, equal (h/a) and (r_1/a). In order to determine the value of h, the visible flame zone was taken to correspond to the peak temperature location [5].

Radiative Heat Flux Calculations

Three measurements, (at the centerline and at two off-center locations) were used to determine the radiative energy emitted through the top and bottom surfaces of the cylindrical control volume in the following manner:

$$Q_r = 2\pi\left(\oint_{A_{ox}} q_{ox}(r, z = 0) r\, dr + \oint_{A_{fu}} q_{fu}(r, z = L) r\, dr\right). \quad (3)$$

The RHS of Eq. 3 represents the radiative flux emitted through the oxidizer duct and the fuel duct respectively. In Eq. 3, q is the measured heat flux at radial locations r, A is the relevant control volume area, and the subscripts ox and fu refer to the oxidizer and fuel sides. Likewise, the radiative flux lost through the side of the control volume involves integration with respect to the axial direction:

$$Q_z = 2\pi R_3\left(\int_0^{L_1} q_z(z)\, dz + \int_{L_1}^{L} q_z(z)\, dz\right), \quad (4)$$

where the two terms on the RHS represent the radiative energy emitted radially on fuel and oxidizer side of the visible flame. In Eq. 4, L denotes the separation between the two ducts, L_1 the displacement of the flame from the oxidizer duct, and q_z the measured heat flux leaving the side of the cylindrical control volume at axial stations corresponding to a displacement z. $R_3 (= 60$ mm) represents the radius of the cylindrical control volume. To perform the integration, polynomial fits were obtained for q_{ox} and q_{fu} versus r, and for q_z versus z.

Global Heat Release

The integrated global heat release rate Q arising from within a stream tube is [26]

$$Q = \int_0^L q_n(z) A(z)\, dz, \quad (5)$$

where $q_n(z)$ denotes the local net heat release rate obtained from summing the heat release for each of the 357 chemical reactions in the simulation, and $A(z)$ is the local stream tube area ratio. The value of A is based on the global continuity equation [27], namely,

$$\rho v A = \rho_{ox/fu} v_{ox/fu}. \quad (6)$$

In Eq. 6, ρ denotes the density, v the velocity, and the subscripts ox and fu refer, respectively, to conditions at the oxidizer and fuel ducts.

RESULTS AND DISCUSSION

The equilibrium heat release Q_{eq} was calculated assuming a one-step reaction in which fuel and oxidizer react to form the products CO_2 and H_2O in the case of methane, and CO_2, H_2O, and HCl in the case of chloromethane. The thermodynamic data for this calculation were obtained from Ref. 28. The equilibrium heat release rate was obtained on the basis of the oxidizer flowrate, since the overall stoichiometry was such that the flame was oxygen limited. The nonpremixed flame calculations were straightforward. For the

flame inhibited with chloromethane on the oxidizer side, a lean premixed flame was first considered, followed by a nonpremixed flame. The amount of oxidizer associated with the two reaction zones differed, since a larger oxygen flowrate was available to the lean premixed flame than to the nonpremixed flame.

In Table 2 the equilibrium and global heat release rates are presented in the context of Eq. 5, as well as the integrated volumetric heat release rate calculated for a uniform stream tube (i.e., $A = 1$). Significant errors can arise if the value of A is miscalculated. Table 2 shows that the global heat release decreased as inhibitors were added to the oxidizer stream, but increased when chloromethane was added to the fuel stream of the nonpremixed flame.

Table 3 presents the spatially integrated net (sum of forward and backward) heat release rates integrated along the axis of symmetry $\int_0^L q_R(z)\,dz$ corresponding to the significant exothermic reactions for flames with 13% N_2 and 9% CH_3Cl added to the oxidizer stream (flames 3 and 5 in Table 2), and for 50% CH_3Cl added to the fuel stream (flame 6 in Table 2), where q_R denotes the local volumetric heat release rate. Consideration of the *net* heat release rates of key reactions allowed evaluation of the relative importance of a particular reaction pathway to flame energetics. For ease of presentation, discussion of a particular reaction refers to the net sum of the forward minus backward rates.

Addition of nitrogen inhibited the flames by decreasing the temperature and thereby diminishing the heat release from reactions R217, R211, R221, R113, R185, R141, R235, and R219 (see Table 3). Dilution with nitrogen decreased both the local temperature and the relative concentrations of the species participating in these reactions:

$$H + O_2 + M_4 \rightarrow HO_2 + M_4, \quad \text{(R217)}$$

$$OH + H_2 \rightarrow H_2O + H, \quad \text{(R211)}$$

$$H + HO_2 \rightarrow OH + OH, \quad \text{(R221)}$$

$$CO + OH \rightarrow CO_2 + H, \quad \text{(R113)}$$

$$O + HCCO \rightarrow H + CO + CO, \quad \text{(R185)}$$

$$C_2H_2 + O \rightarrow CH_2 + CO, \quad \text{(R141)}$$

$$H + OH + M_6 \rightarrow H_2O + M_6, \quad \text{(R235)}$$

$$CH_3 + O \rightarrow CH_2O + H. \quad \text{(R19)}$$

Though R113 and R211 had relatively large integrated heat release rates, the backward rates involving these reactions were also large, yielding a net rate that was relatively small.

Table 3 shows that with the addition of 9% CH_3Cl to the oxidizer stream, the key reactions controlling the heat release were R299 and R305. Reaction R305 can be thought of as analogous to R211 in the base flame.

$$H + Cl + M \rightarrow HCl + M, \quad \text{(R299)}$$

$$OH + HCl \rightarrow Cl + H_2O. \quad \text{(R305)}$$

There were two distinct combustion regions in the flame established with the addition of 9% CH_3Cl to the oxidizer stream, namely, an oxidizer-side premixed type zone and a fuel-side nonpremixed type zone. Though the inhibitor was added to the oxidizer stream, reactions R299, R305, and R113 were dominant on

TABLE 2

The Equilibrium, Global Heat Release Rates, and Integrated Volumetric Heat Release Rates Calculated for a Uniform Stream Tube Ratio

Flame	Added to	Q_{eq} (W m^{-2})	Q (W m^{-2})	$\int_0^L q_n\,dz$ (W m^{-2})
(1) CH_4–Air	—	$2.39 \cdot 10^6$	$2.51 \cdot 10^6$	$2.68 \cdot 10^5$
(2) +6.6% N_2	oxidizer	$2.29 \cdot 10^6$	$2.40 \cdot 10^6$	$2.55 \cdot 10^5$
(3) +13% N_2	oxidizer	$2.11 \cdot 10^6$	$2.27 \cdot 10^6$	$2.42 \cdot 10^5$
(4) +5% CH_3Cl	oxidizer	$2.22 \cdot 10^6$	$2.21 \cdot 10^6$	$3.03 \cdot 10^5$
(5) +9% CH_3Cl	oxidizer	$2.12 \cdot 10^6$	$1.19 \cdot 10^6$	$3.34 \cdot 10^5$
(6) +50% CH_3Cl	fuel	$2.57 \cdot 10^6$	$3.04 \cdot 10^6$	$2.42 \cdot 10^5$

TABLE 3

Significant Net Heat Release Rates Associated with *Exothermic* Reactions (in units of J s^{-1} m^{-2})[a]

		Base Flame	+13% N_2	+9% CH_3Cl	+50% CH_3Cl
(R19)	$CH_3 + O \rightarrow CH_2O + H$	$-1.20 \cdot 10^4$	$-1.29 \cdot 10^4$	$-1.75 \cdot 10^4$	$-8.62 \cdot 10^3$
(R113, 114)	$CO + OH \rightarrow CO_2 + H$	$-2.29 \cdot 10^4$	$-2.14 \cdot 10^4$	$-3.26 \cdot 10^4$	$-2.31 \cdot 10^4$
(R141)	$C_2H_2 + O \rightarrow CH_2 + CO$	$-1.74 \cdot 10^4$	$-1.42 \cdot 10^4$	$-1.03 \cdot 10^4$	$-1.54 \cdot 10^4$
(R153)	$C_2H_3 + O_2 \rightarrow CH_2O + HCO$	*	*	$-2.05 \cdot 10^4$	*
(R185)	$O + HCCO \rightarrow H + CO + CO$	$-2.01 \cdot 10^4$	$-1.67 \cdot 10^4$	*	$-1.62 \cdot 10^4$
(R211, 212)	$OH + H_2 \rightarrow H_2O + H$	$-3.81 \cdot 10^4$	$-3.33 \cdot 10^4$	$-1.35 \cdot 10^4$	$-1.97 \cdot 10^4$
(R217)	$H + O_2 + M_4 \rightarrow HO_2 + M_4$	$-5.87 \cdot 10^4$	$-4.76 \cdot 10^4$	*	$-1.94 \cdot 10^4$
(R221)	$H + HO_2 \rightarrow OH + OH$	$-2.94 \cdot 10^4$	$-2.52 \cdot 10^4$	*	*
(R235)	$H + OH + M_6 \rightarrow H_2O + M_6$	$-1.59 \cdot 10^4$	*	*	*
	Cl-Related Chemistry				
(R257, 258)	$CH_3Cl + Cl \rightarrow CH_2Cl + HCl$	—	—	$-8.00 \cdot 10^3$	*
(R259)	$CH_3Cl + H \rightarrow CH_3 + HCl$	—	—	*	$-5.49 \cdot 10^3$
(R279)	$CH_2Cl + OH \rightarrow CH_2O + HCl$	—	—	$-1.52 \cdot 10^4$	*
(R281)	$CH_2O + Cl \rightarrow HCO + HCl$	—	—	$-1.68 \cdot 10^4$	*
(R285)	$CH_3 + CH_2Cl \rightarrow C_2H_4 + HCl$	—	—	$-1.01 \cdot 10^4$	*
(R299)	$H + Cl + M \rightarrow HCl + M$	—	—	$-1.15 \cdot 10^5$	$-8.21 \cdot 10^4$
(R305, 306)	$OH + HCl \rightarrow Cl + H_2O$	—	—	*	$-9.74 \cdot 10^3$
(R341)	$CH_2Cl + H \rightarrow CH_3 + Cl$	—	—	$-1.58 \cdot 10^4$	*

[a] The symbol * signifies a heat release rate that is less than 10^3 J s^{-1} m^{-2}. The presence of both forward and backward reactions in brackets ($R_{(forward)}$, $R_{(backward)}$) indicates that the rates of both are relatively large. The subscripts i with respect to the third bodies M_i represent different third body efficiencies [22].

the fuel side, whereas R153 was important on the oxidizer side of the flame.

$$C_2H_3 + O_2 \rightarrow CH_2O + HCO. \qquad \text{(R153)}$$

Reactions of secondary importance to the heat release included R281, R341, R279, and R285 with maxima in the premixed region, and R19, R211, and R141 in the nonpremixed region (in order of decreasing magnitude).

$$CH_2O + Cl \rightarrow HCl + HCO, \qquad \text{(R281)}$$

$$CH_2Cl + H \rightarrow CH_3 + Cl, \qquad \text{(R341)}$$

$$CH_2Cl + OH \rightarrow CH_2O + HCl, \qquad \text{(R279)}$$

$$CH_3 + CH_2Cl \rightarrow C_2H_4 + HCl, \qquad \text{(R285)}$$

$$CH_3 + O \rightarrow CH_2O + H, \qquad \text{(R19)}$$

$$OH + H_2 \rightarrow H_2O + H, \qquad \text{(R211)}$$

$$C_2H_2 + O \rightarrow CH_2 + CO. \qquad \text{(R141)}$$

The *net* heat release associated with the CO burnout reaction (R113) rose, since CO is formed on both sides of the high temperature reaction zone. Chlorine is abstracted from chloromethane, and as a result CH_3 radicals were available for the formation of C_2 containing species [22]. The increased role of the C_2-related chemistry was evident from the relative importance of R153 when CH_3Cl was added to the oxidizer stream.

When chloromethane was added to the fuel stream the heat release due to R299 and R305 was larger than that due to reactions R217 and R211 which, though diminished, remained significant sources of heat release.

$$H + Cl + M \rightarrow HCl + M, \qquad \text{(R299)}$$

$$OH + HCl \rightarrow Cl + H_2O, \qquad \text{(R305)}$$

$$H + O_2 + M_4 \rightarrow HO_2 + M_4, \qquad \text{(R217)}$$

$$OH + H_2 \rightarrow H_2O + H. \qquad \text{(R211)}$$

R221 and R235 were no longer significant whereas the heat release associated with HO_2 consumption occurred mainly through R309.

$$H + HO_2 \rightarrow OH + OH, \qquad \text{(R221)}$$

$$H + OH + M_6 \rightarrow H_2O + M_6, \qquad \text{(R235)}$$

$$Cl + HO_2 \rightarrow HCl + O_2. \qquad \text{(R309)}$$

Thus, chlorine chemistry was of primary importance in terms of the heat release when chloromethane was added to the fuel stream (cf. R299 and R305) and the reactions associated with oxidation of methane took on a secondary importance (cf. R211, R217). Heat release due to the CO burnout reaction (R113) was not significantly perturbed by addition of chloromethane to the fuel stream.

Table 4 contains a list of the significant endothermic reactions for a number of the flames, and the values of their net (sum of forward and backward) heat release rates spatially integrated along the axis of symmetry. The important endothermic reactions in the base flame (in order of decreasing value) were R214, R136, R148, and R101, with the first three of the same order of magnitude.

$$O_2 + H \rightarrow O + OH, \qquad \text{(R214)}$$

$$C_2H_5 + M_1 \rightarrow H + C_2H_4 + M_1, \qquad \text{(R136)}$$

$$C_2H_3 + M_1 \rightarrow H + C_2H_2 + M_1, \qquad \text{(R148)}$$

$$HCO + M_2 \rightarrow H + CO + M_2. \qquad \text{(R101)}$$

Addition of nitrogen decreased the endothermicity (by decreasing both the specific reaction rate constants through a decrease in temperature, and by diluting the relative concentrations of the reacting species), but not the ordering of the endothermic reactions. The same endothermic reactions were important when chloromethane was added to the flame, regardless of which side the addition occurred. Upon addition of 9% CH_3Cl to the oxidizer stream the reactions R214, R136, R101, and R148 were still the key endothermic processes (listed in decreasing magnitude). There were no reactions involving chlorinated species that competed with these key reactions. Reaction R101 became a major channel for CO formation, since O atoms were depleted on the oxidizer side of the high temperature reaction zone, thereby suppressing the role of R185.

$$O + HCCO \rightarrow H + CO + CO. \qquad \text{(R185)}$$

In addition, reactions R226 and R4 were key contributors to the endothermicity.

$$O + H_2O \rightarrow OH + OH, \qquad \text{(R226)}$$

$$CH_4 + M_1 \rightarrow CH_3 + H + M_1. \qquad \text{(R4)}$$

Endothermicity caused by addition of CH_3Cl to the fuel stream was small, except for increased energy absorption due to R148, the reverse of reaction R225.

$$C_2H_3 + M_1 \rightarrow H + C_2H_2 + M_1. \qquad \text{(R148)}$$

The global heat release profiles associated with the flames are presented in Fig. 3. Addition of nitrogen to the oxidizer stream narrowed the heat release region (consistent with the thermal suppression), though the nature of the profiles was qualitatively similar. Chloromethane addition to the fuel stream altered the flame stoichiometry, and moved the flame closer to the fuel duct. The heat release profiles were markedly different when CH_3Cl was added to the oxidizer stream, with large

TABLE 4

Significant Net Heat Release Rates Associated with *Endothermic* Reactions (in units of J s^{-1} m^{-2})[a]

		Base Flame	+13% N_2	+9% CH_3Cl	+50% CH_3Cl
(R4)	$CH_4 + M_1 \rightarrow CH_3 + H + M_1$	*	*	$1.02 \cdot 10^4$	*
(R101)	$HCO + M_2 \rightarrow H + CO + M_2$	$1.23 \cdot 10^4$	$1.05 \cdot 10^4$	$2.88 \cdot 10^4$	$1.14 \cdot 10^4$
(R135, 136)	$C_2H_5 + M_1 \rightarrow H + C_2H_4 + M_1$	$3.38 \cdot 10^4$	$2.83 \cdot 10^4$	$3.05 \cdot 10^4$	$2.84 \cdot 10^4$
(R148)	$C_2H_3 + M_1 \rightarrow H + C_2H_2 + M_1$	$2.98 \cdot 10^4$	$2.39 \cdot 10^4$	$2.15 \cdot 10^4$	$2.27 \cdot 10^4$
(R213, 214)	$O_2 + H \rightarrow O + OH$	$3.45 \cdot 10^4$	$2.96 \cdot 10^4$	$4.66 \cdot 10^4$	$3.64 \cdot 10^4$
(R225, 226)	$O + H_2O \rightarrow OH + OH$	$4.75 \cdot 10^3$	$4.59 \cdot 10^3$	$1.86 \cdot 10^4$	$1.24 \cdot 10^4$
	Cl-Related Chemistry				
(R251)	$CH_3Cl \rightarrow CH_3 + Cl$	—	—	*	$1.22 \cdot 10^4$

[a] The symbol * signifies a heat release rate that is less than 10^3 J s^{-1} m^{-2}. The presence of both forward and backward reactions in brackets ($R_{(forward)}$, $R_{(backward)}$) indicates that the rates of both are relatively large. The subscripts i with respect to the third bodies M_i represent different third body efficiencies [22].

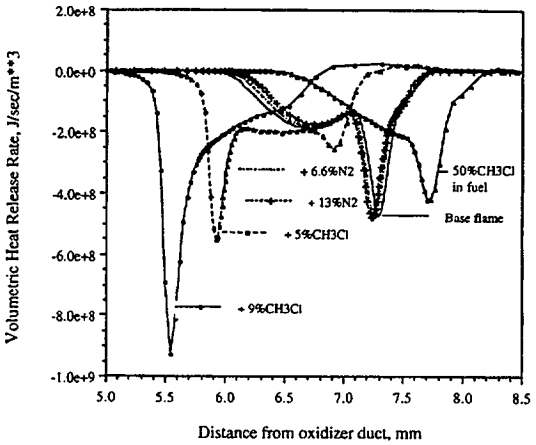

Fig. 3. The heat release profiles of several flames.

amounts of heat release associated with the premixed flame. The heat release was considerably suppressed when the CH_3Cl was raised to 9% by volume.

The smaller region over which the heat release took place in the presence of additional nitrogen lead to a lower net heat release, and thereby decreased the maximum flame temperature as shown in Fig. 4. Figure 4 also shows that chloromethane addition to the fuel stream slightly raised the peak flame temperature, and moved its location towards the fuel duct. The flame temperature profiles were broadened and the peak increased upon chloromethane addition to the oxidizer stream due to the additive enthalpy. The peak temperature location moved closer to the oxidizer duct when CH_3Cl was added to that side in accord with the heat release distribution.

The impact of CH_3Cl addition on the heat release is illustrated in Figs. 5 and 6 where the profiles of significant exothermic reactions are presented. From these profiles it is noted that heat release on the oxidizer side of the flame occurred in a narrow region extending from ≈ 5.3 to ≈ 5.8 mm from the oxidizer duct. There, the chlorine chemistry impacted the heat release through reactions (in order of decreasing magnitude) R341, R279, R285, and R257.

$$CH_2Cl + H \rightarrow CH_3 + Cl, \quad \text{(R341)}$$

$$CH_2Cl + OH \rightarrow CH_2O + HCl, \quad \text{(R279)}$$

$$CH_3 + CH_2Cl \rightarrow C_2H_4 + HCl, \quad \text{(R285)}$$

$$CH_3Cl + Cl \rightarrow CH_2Cl + HCl. \quad \text{(R257)}$$

Significant exothermic reactions that did not involve chlorine were the oxidative reactions R153 and R109. In a broad region extending from ≈ 5.3 to ≈ 6.8 mm the coupled reactions R299 and R305 dominated the heat release through transport of chlorine atoms to the flame. The result of the coupling was radical recombination through the net reaction (R299 + R305):

$$H + OH + Cl \rightarrow H_2O + Cl \quad \text{(R299 + R305)}$$

in which chlorine "catalyzed" chain termination. The exothermicity of the two reactions is

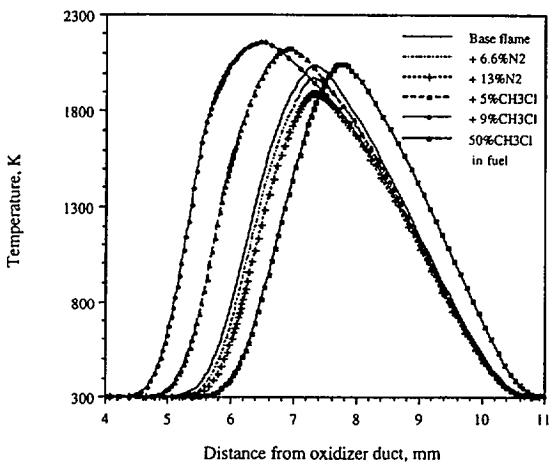

Fig. 4. The temperature profiles of several flames.

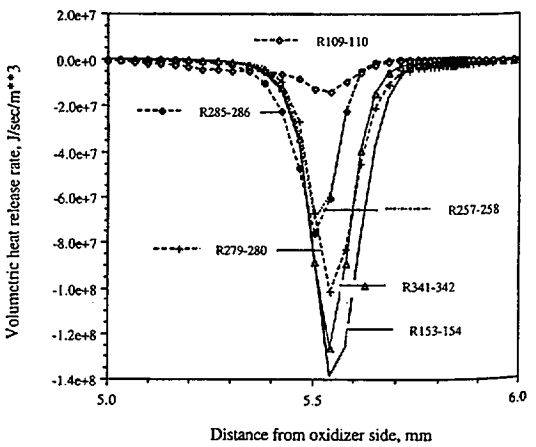

Fig. 5. The heat release profiles of some significant exothermic reactions in flame 5 (see Table 2).

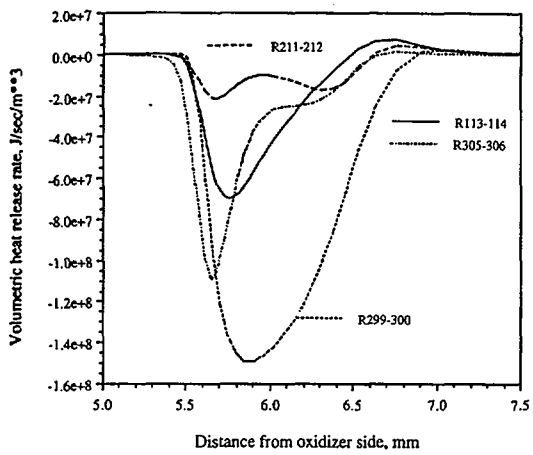

Fig. 6. The heat release profiles of other significant exothermic reactions in flame 5 (see Table 2).

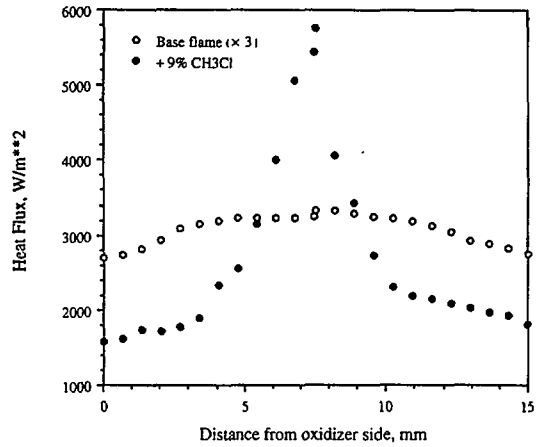

Fig. 7. The measured radiative heat flux profiles measured along R_3 (see Fig. 2).

also coupled through the CO burnout reaction R113. Chloromethane addition to the fuel stream did not exhibit as strong a coupling between reactions R299 and R305, since there were other competing exothermic pathways for OH consumption through R113, R211, R213, and R225.

$$CO + OH \rightarrow CO_2 + H, \qquad \text{(R113)}$$

$$OH + H_2 \rightarrow H_2O + H, \qquad \text{(R211)}$$

$$O + OH \rightarrow O_2 + H, \qquad \text{(R213)}$$

$$OH + OH \rightarrow O + H_2O. \qquad \text{(R225)}$$

Radiation

Figure 7 shows the radiative heat flux measurements along R_3, parallel to the axis of symmetry (see Fig. 2), for flames 1 and 5 of Table 2. The flux had a maximum near the duct center, where the highest flame temperatures occurred. The flux emitted along R_3 for the flame with 9% chloromethane added on the oxidizer side was several times larger than that emitted by the base flame, as shown. Table 5 presents the measured radiative flux determined by summing Eqs. 3 and 4 for the five flames. The bulk of the thermal radiation was lost through the circular ducts rather than the sides of the cylindrical control volume. In general, the fuel-side duct accounted for a larger loss of radiative energy than does the oxidizer side. Calculations using RADCAL [29] employing the simulated flame structure of the base flame substantiated the result that a higher radiative flux occurred towards the fuel duct than towards the oxidizer duct. This result can be attributed to the larger concentrations of radiating gas species (primarily water vapor and carbon dioxide) on the fuel side of the high temperature reaction zone in accord with the results reported in Ref. 13.

In order to estimate the heat release, the global continuity equation must be applied separately to either side of the stagnation plane. The global heat release rate $(Q_{n-A}|_e)$ due to the flame is [26]

$$Q_{n-A}|_e = A_D \int_0^L q_n(z) A(z)\, dz. \qquad (7)$$

In Eq. 7, $q_n(z)$ denotes the local heat release rate obtained from Fig. 3, A_D is the duct area and $A(z)$ was defined previously. Since most of the heat release occurred in the vicinity of the flame an approximate total heat release rate $Q_{n-A}|_a$ is obtained by multiplying the integrated axial heat release rate with the stream tube area at the flame location:

$$Q_{n-A}|_a = A_D A_{st} \int_0^L q_n(z)\, dz, \qquad (8)$$

where the subscript "st" refers to the location of maximum temperature. In the context of Eqs. 7 and 8, the subscripts a and e refer, respectively, to the approximate and exact methods.

TABLE 5

The Measured Emitted Heat Flux Calculated by Application of Eqs. 3 and 4 for the Five Flames

	Measured Radiative Flux (W)				
	Oxidizer Side		Fuel Side		
Flame	Radial	Axial	Radial	Axial	Total
(1) CH_4–Air	10.8	2.7	17.3	3.0	33.8
(2) +6.6% N_2	9.8	2.4	13.9	2.6	28.7
(3) +13% N_2	9.6	2.2	11.2	2.5	25.5
(4) +5% CH_3Cl	14.8	3.2	21.3	4.2	43.5
(5) +9% CH_3Cl	23.1	4.7	27.7	6.0	61.5

The diameter associated with the flame surface area calculated from Eq. 6 is much larger than the observed diameter of the visible flame (shown in Fig. 2) due to quenching of the flame edge by the curtain flow of nitrogen. Therefore, in order to estimate the total *experimental* heat release rate, the stream tube area ratio was assumed to attain a maximum value equal to the area corresponding to the surface of the visible flame A_{vf}, i.e., $A(z)$ was bounded between 1 and A_{vf}/A_D. Thus, the integrated heat release rate, $Q_{n-vf}|_e$, corresponding to the experiment was obtained.

Radiative Emission

The stream tube area ratio at the location of maximum flame temperature, obtained by applying the global continuity equation is presented for the five flames in Table 6. Since the flame moved towards the oxidizer stream upon chloromethane addition, the velocity there was higher and the area ratio lower. The characteristic flame surface area was about 30% smaller for flame 5 when chloromethane was added as compared with flame 3 when nitrogen was added.

Table 6 also presents results for the heat release calculated using the methods described above. For all flames, the nonequilibrium heat release rate $Q_{n-A}|_e$ is within 5% of that calculated assuming chemical equilibrium Q_{eq}. The approximate global heat release $Q_{n-A}|_a$ calculated using Eq. 8 is as much as 15% larger than the heat release, $Q_{n-A}|_e$, calculated using Eq. 7. The approximation did somewhat better for flames near extinction (flames 3 and 5). The heat release rate, $Q_{n-vf}|_e$, corresponding to the experiment is approximately a factor of 3 less than $Q_{n-A}|_e$, due to quenching of the flame edge by the nitrogen curtain.

Whichever method was used to calculate the heat release, addition of nitrogen decreased that value, primarily by decreasing the amount of oxygen available to the flame. Although the chloromethane flames (flames 4 and 5) were

TABLE 6

The Stream Tube Area Ratio A_{st} at the Maximum Flame Temperature, Displacement of the Peak Temperature Location from the Oxidizer Duct L_1, Heat Release Based on (a) Chemical Equilibrium Q_{eq}, (b) the Numerical Simulations and the Stream Tube Area Q_{n-A}, and (c) the Numerical Simulations and the Visible Flame Area Q_{n-vf} (the subscripts $-e$ and $-a$ refer to the exact and approximate methods discussed in the text), and the Fractional Radiative Flux χ_R based on $Q_{n-vf}|_e$ Expressed in Percent

			Heat Release (W)				
Flame	A_{st}	L_1 (mm)	Q_{eq}	$Q_{n-A}\|_e$	$Q_{n-A}\|_a$	$Q_{n-vf}\|_e$	χ_R (%)
(1) CH_4/Air	10.5	7.3	4330	4550	5090	1420	2.4
(2) +6.6% N_2	10.5	7.3	4150	4340	4830	1350	2.1
(3) +13% N_2	10.4	7.3	3810	4100	4530	1280	2.0
(4) +5% CH_3Cl	8.5	6.9	4020	4010	4640	1600	2.7
(5) +9% CH_3Cl	6.9	6.5	3840	3600	4180	1770	3.5

closer to extinction, they had a higher heat release rate ($Q_{n-vf}|_e$) than the uninhibited base flame (flame 1).

The fractional radiative loss from the flame χ_R was determined by comparing the measured radiative flux with the total heat release rate based on $Q_{n-vf}|_e$. The χ_R values so calculated are tabulated in Table 6. For the base case (flame 1), χ_R is in good agreement with the value (= 0.02) calculated in Ref. 14 for moderately strained (100 s^{-1}) methane/air nonpremixed flames. As nitrogen was added to the oxidizer stream, the radiative heat loss fraction decreased slightly. This is consistent with the view that for flames near extinction, either through stretch or dilution with N_2, the radiative heat loss should diminish as the peak flame temperature decreases and the reaction zone narrows [14, 15]. For flames to which a halogenated inhibitor was added to the oxidizer stream, the radiative emission increased (see Table 5) and so did the radiative heat loss fraction (Table 6).

In general, values of χ_R do not differ much, taking on values from 2.0 to 3.5% for the five flames. This leads us to conclude that radiative losses do not significantly contribute towards extinction of *moderately* stretched flames, and that our simulations are reasonably accurate. However, analyses of extinguishment processes should consider radiation losses particularly if substantial amounts of particulates are present in the flames.

CONCLUSIONS

The chemical and thermal structure of inhibited flames was investigated in order to characterize the effects due to inhibition on the heat release.

- In general, when inhibitors were added to the oxidizer stream of a nonpremixed flame, the global heat release decreased. However, chloromethane addition to the fuel stream increased the heat release. Whereas addition of nitrogen narrowed the heat release region, chloromethane addition to the oxidizer altered the flame structure, such that two distinct heat release regions were present.
- Halogen addition to the oxidizer stream of flames introduced substitute pathways to supplement those by which the heat release occurred (e.g., R299 and R305 in addition to R217 and R211). Though inhibition effects occurred in a premixed-like region on the oxidizer side of the high temperature reaction zone, the effects of mass diffusion and thermochemistry were such that halogen-involving heat release reactions were dominant on the fuel side.
- Compared with the chemistry associated with hydrocarbon burning, halogenated channels were the dominant heat release paths when chloromethane was added to the fuel stream. Furthermore, the CO burnout reaction was not significantly perturbed by addition of chloromethane to the fuel stream of the base flame.
- Halogen addition to either side of the flame did not significantly affect the endothermic pathways.
- Chloromethane addition to the oxidizer resulted in a coupling of the premixed and nonpremixed flame regions through the net reaction $H + OH + Cl \rightarrow H_2O + Cl$.
- Radiative heat flux measurements obtained in moderately strained counterflow diffusion flames showed that:
  - As nitrogen was added to the "base" flame, the radiative heat loss fraction decreased somewhat (< 20%), whereas when a halogenated inhibitor was added to that flame, the radiative heat loss fraction increased substantially (> 80%).
  - The fractional radiative flux emitted from these moderately strained flames was very small in comparison with the total flame heat release and the radiative flux did not significantly contribute towards flame extinction. Thus, numerical simulations of flame structure can reasonably neglect emission from such moderately strained flamelets.

The authors thank Dr. M. H. Yang of UIC for several helpful discussions. Further details regarding the methodology are to be found in Ref. 30.

REFERENCES

1. Chang, W. D., Karra, S. B., and Senkan, S. M., *Combust. Flame* 69:113–122 (1987).

2. Karra, B., Gutman, D., and Senkan, S. M., *Combust. Sci. Technol.* 60:45–62 (1988).
3. Pitz, W. J., and Westbrook, C. K., Presented at the Western States Section/The Combustion Institute held at La Jolla, California, 1990.
4. Barat, R. B., Sarofim, A. F., Longwell, J. P., and Bozzelli, J. W., *Combust. Sci. Technol.* 74:361–378 (1990).
5. Yang, M. H., Hamins, A., and Puri, I. K., *Combust. Flame* 98:107–122 (1994).
6. Huh, J. Y., Lee, K. Y., and Puri, I. K., *Combust. Flame* 96:381–392 (1994).
7. Yang, M. H., and Puri, I. K., *Combust. Flame* 94:25–34 (1993).
8. Dixon-Lewis, G., David, T., Gaskell, P. H., Fukutani, S., Jinno, H., Miller, J. A., Kee, R. J., Smooke, M. D., Peters, N., Effelsburg, E., Warnatz, J., and Behrendt, F., *Twentieth Symposium (International) on Combustion*, The Combustion Institute, Pittsburgh, 1984, pp. 1893–1904.
9. Smooke, M. D., and Giovangigli, C. V., In *Reduced Kinetic Mechanisms and Asymptotic Approximations for Methane–Air Flames* (M. D. Smooke, Ed.), Springer Verlag, Berlin, 1991, pp. 1–28.
10. Rogg, B., University of Cambridge, Report CUED/A-THERMO/TR39, April 1991.
11. Sohrab, S. H., Linan, A., and Williams, F. A., *Combust. Sci. Technol.* 27:143–154 (1982).
12. Abdel-Khalik, S., Tamaru, T., and El-Wakil, M. M., *Heat Transfer in Flames* (N. H. Afgan and J. M. Beer, Eds.), Scripta, Washington D.C., 1974, Chap. 23.
13. Hall, R. J., *J. Quant. Spectrosc. Radiat. Transf.* 49:517–523 (1993).
14. Vranos, A., and Hall, R. J., *Combust. Flame* 93:230–238 (1993).
15. Chan, S. H., Pan, X. C., and Abou-Ellail, M. M. M., Presented at the Eastern States Section Meeting of the Combustion Institute held at Princeton, NJ, October 25–27, 1993.
16. Williams, F. A., *Combustion Theory*, Benjamin/Cummings, Menlo Park, CA, 1985.
17. Chelliah, H. K., Law, C. K., Ueda, T., Smooke, M. D., and Williams, F. A., *Twenty-Third Symposium (International) on Combustion*, The Combustion Institute, Pittsburgh, 1990, pp. 503–511.
18. Hamins, A., Thridandam, H., and Seshadri, K., *Chem. Eng. Sci.* 40:2027–2038 (1985).
19. Puri, I. K., Ph.D. thesis, University of California, San Diego, 1987.
20. Rogg, B., In *Computers and Experiments in Fluid Flow* (G. M. Carlomagno and C. A. Brebbia, Eds.), Springer-Verlag, Berlin, 1989, pp. 75–85.
21. Miller, J. A., and Bowman, C. T., *Prog. Ener. Combust. Sci.* 15:287–338 (1989).
22. Lee, K. Y., Yang, M. H., and Puri, I. K., *Combust. Flame* 92:419–439 (1992).
23. McCaffrey, B. J., Presented at the Meeting of the Western States Section of the Combustion Institute held in 1981.
24. Hamins, A., Klassen, M., Gore, J., and Kashiwagi, T., *Combust. Flame* 86:223–228 (1991).
25. Howell, J. R., A *Catalog of Radiation Configuration Factors*, McGraw-Hill, New York, 1982, pp. 32–33.
26. Fristrom, R. M., and Westenberg, A. A., *Flame Structure*, McGraw-Hill, New York, 1965.
27. Tsuji, H., and Yamaoka, I., *Thirteenth Symposium (International) on Combustion*, The Combustion Institute, Pittsburgh, 1970, pp. 723–731.
28. Chase, M. W., Davies, C. A., Downey, J. R., Frurip, D. J., MacDonald, R. A., and Syverud, A. N., *JANAF Thermochemical Tables*, 3rd ed., ACS and AIP for NBS, 1985, 14.
29. Grosshandler, W. L., *RADCAL: A Narrow-Band Model for Radiation Calculations in a Combustion Environment*, U.S. Government Printing Office, NIST Publication 1402, 1993.
30. Lee, K. Y., Flame Structure Studies Applied to Inhibition, Extinction, and Pollutant Formation, Ph.D. Thesis, University of Illinois at Chicago, Chicago, 1995.

Received 14 July 1994; revised 7 April 1995